

Charge Transport in DNA Oligonucleotides with Various Base-Pairing Patterns

Irena Kratochvílová,^{*,†} Tatiana Todorciuc,[†] Karel Král,[†] Hynek Němec,[†] Martin Bunčák,[‡] Jakub Šebera,^{§,||} Stanislav Záliš,^{||} Zuzana Vokáčová,[⊥] Vladimír Sychrovský,[⊥] Lucie Bednářová,[⊥] Peter Mojžeš,[#] and Bohdan Schneider^{*,†,∇}

Institute of Physics AS CR, v.v.i., Na Slovance 2, CZ-182 21 Prague 8, GENERI BIOTECH s.r.o., Machkova 587, CZ-500 11 Hradec Králové, Institute of Macromolecular Chemistry AS CR, v.v.i., Heyrovského nám. 2, CZ-162 06 Prague 6, J. Heyrovský Institute of Physical Chemistry AS CR, v.v.i., Dolejškova 3, CZ-182 23 Prague 8, Gilead Sciences and IOCB Research Center, Institute of Organic Chemistry and Biochemistry AS CR, v.v.i., Flemingovo sq. 2, CZ-166 10 Prague 6, Institute of Physics, Faculty of Mathematics and Physics, Charles University in Prague, Ke Karlovu 5, CZ-121 16 Prague 2, and Institute of Biotechnology AS CR, v.v.i., Vídeňská 1083, CZ-142 20 Prague 4, Czech Republic

Received: January 11, 2010; Revised Manuscript Received: March 4, 2010

We combined various experimental (scanning tunneling microscopy and Raman spectroscopy) and theoretical (density functional theory and molecular dynamics) approaches to study the relationships between the base-pairing patterns and the charge transfer properties in DNA 32-mer duplexes that may be relevant for identification and repair of defects in base pairing of the genetic DNA and for DNA use in nanotechnologies. Studied were two fully Watson–Crick (W-C)-paired duplexes, one mismatched (containing three non-W-C pairs), and three with base pairs chemically removed. The results show that the charge transport varies strongly between these duplexes. The conductivity of the mismatched duplex is considerably lower than that of the W-C-paired one despite the fact that their structural integrities and thermal stabilities are comparable. Structurally and thermally much less stable abasic duplexes have still lower conductivity but not markedly different from the mismatched duplex. All duplexes are likely to conduct by the hole mechanism, and water orbitals increase the charge transport probability.

1. Introduction

The protection of genetic information, the fundamental biological function of the DNA molecule, is dependent on infallible matching of complementary bases in the Watson–Crick (W-C) pairs, and any errors in their recognition may lead to the production of nonfunctional or even harmful RNA or protein. The detection of the occurrence of non-W-C or otherwise damaged or missing base pairs by cellular checking and repair mechanisms is therefore of vital importance. However, base pairing and its manifestations may not be of importance only for biology, because the self-assembling ability of DNA is also of great interest for material science where various nanoscale objects could be constructed from properly designed self-assembling oligonucleotides.

This work studies the consequences of structural perturbations on charge transport in double-helical oligonucleotide DNA caused by mismatched or missing base pairs. Charge transport along or through DNA molecules has been investigated by various experimental techniques for over a decade, sometimes with contradictory results,^{1–11} so that understanding of the charge transport through a polyelectrolyte aperiodic system as complicated as double-helical DNA continues to be a major scientific problem. Several mechanisms may contribute to the charge

transport in DNA, namely, electronic conduction along base pair sequences, ionic conduction associated with the counterions at the solvation shell surrounding the duplex, reorientation of the water dipoles around the duplex,^{12–14} and also phonons resulting from the structural fluctuations of the duplex.^{15,16}

Charge migration along DNA double-helical molecules may be of biological importance as the extended electronic states of DNA could play a role in the processes of sensing and/or repair of DNA damage.^{1,17–21} Barton and co-workers have brought firm evidence that the double helix can serve as a bridge for electron transfer²² and that rhodium intercalator noncovalently bound to the duplex can catalyze repair of a thymine covalent dimer, a common DNA lesion, at a distance of a few nanometers, and that this long-range repair is mediated by hole transfer through the DNA helix.^{23,24} Guanine, especially in short sequences, has the smallest oxidation potential of all of the natural bases, and Heller¹⁹ hypothesized that guanine-rich regions may function as a cathodic protection of long DNA stretches. Localization of oxidative damage has been studied at steps containing guanine and other bases, and charge transfer has been clearly shown to be sequence-dependent.^{17,25–28} Quite significantly, a DNA duplex with non-W-C pairs can be recognized by its different electrical behavior,²⁹ for example, by its much lower conductivity than that of a fully W-C-paired duplex.³⁰

We combined various experimental techniques [scanning tunneling microscopy (STM) and Raman spectroscopy] and theoretical approaches [molecular dynamics (MD) and quantum mechanics] to investigate the relationship between structural, electronic, and charge transport properties of six types of double-helical oligonucleotides: two duplexes with the “canonical” W-C pairs and duplexes containing two types of DNA lesions, one

* To whom correspondence should be addressed. E-mail: krat@fzu.cz (I.K.) or bohdan@img.cas.cz (B.S.).

[†] Institute of Physics AS CR.

[‡] GENERI BIOTECH s.r.o.

[§] Institute of Macromolecular Chemistry AS CR.

^{||} J. Heyrovský Institute of Physical Chemistry AS CR.

[⊥] Institute of Organic Chemistry and Biochemistry AS CR.

[#] Charles University in Prague.

[∇] Institute of Biotechnology AS CR.

TABLE 1: Investigated DNA Double Helical Samples^a

label	sequence	GC/AT	experiments
STANDARD	5'-GTTAGCACGATAGTCCGATAGTCAGTCAGTCC-3' 3'-CAATCGTGCTATCAGGCTATCAGTCAGTCAGG-5'	16GC/16AT	STM, Raman
STANDARD GC	5'-CGGCAGCGGCAGGCGTGTGGGCGTCGGTCGTT-3' 3'-GCCGTCGCCGTCGCCACACCCGCAGCCAGCAA-5'	24GC/8AT	STM, Raman
MSMCH3	5'-GTTAGCACGATAGTCCGATAGTCAGTCAGTCC-3' 3'-CAATCGTGCTATCACCTTATCAGTCAGTCAGG-5'	13GC/16AT 3 mismatch	STM, Raman
ABASIC3	5'-GTTAGCACGATAGTXXXATAGTCAGTCAGTCC-3' 3'-CAATCGTGCTATCAXXXTATCAGTCAGTCAGG-5'	13GC/16AT (3 abasic)	STM
ABASIC4	5'-GTTAGCACGATAGXXXXATAGTCAGTCAGTCC-3' 3'-CAATCGTGCTATCXXXXTATCAGTCAGTCAGG-5'	13GC/15AT (4 abasic)	STM, Raman
ABASIC5	5'-GTTAGCACGATAXXXXXATAGTCAGTCAGTCC-3' 3'-CAATCGTGCTATXXXXTATCAGTCAGTCAGG-5'	12GC/15AT (5 abasic)	STM, Raman

^a The column "experiments" provides the experimental techniques used to measure the particular sample.

containing mismatched base pairs and three with a few bases removed so that three, four, or five of their base pairs were missing. Exploration of the relationships between structural consequences of a particular modification in the DNA base-pairing pattern and its charge transport properties is apparently complex, but their elucidation may help explain the biological significance of charge transfer through DNA as well as facilitate DNA utilization in nanotechnology.

2. Materials and Methods

The following paragraphs detail the DNA samples studied as well as their preparation (section 2.1) and describe the techniques used (section 2.2).

2.1. Materials. Six 32-nucleotide-long DNA duplexes of various sequences and base-pairing patterns were studied (Table 1). The STANDARD duplex was assembled from two complementary single-stranded 32-mers containing all four types of nucleotides in an equal proportion and in quasi-random nonself complementary sequences restricting the formation of intrastrand loops. This duplex served as the basic oligonucleotide model of natural DNA, and its conductivity and structural properties were compared to other 32-mer duplexes. The other canonical duplex had an increased G-C content (STANDARD GC), and the remaining four samples had impaired or missing W-C pairing: One duplex contained three mismatched base pairs (MSMCH3), and three duplexes had three, four, and five base pairs, respectively, eliminated from their central parts (ABASIC3, ABASIC4, and ABASIC5).

All of the duplexes were prepared from single-stranded oligonucleotides synthesized in an ABI394 synthesizer using standard phosphoramidite chemistry.^{31–33} The standard base phosphoramidites (for A, G, C, and T) and dSpacer CE Phosphoramidite (for abasic sites) were purchased from Glen Research (United States) and used according to the manufacturer's recommendations. Single-stranded oligonucleotides were purified by reverse-phase chromatography and analyzed by high-performance liquid chromatography (HPLC) and matrix-assisted laser desorption/ionization time-of-flight (MALDI-TOF) for quality control. The purity of all of the sequences was >98% according to the HPLC and MALDI-TOF analyses.

The duplexes for Raman spectroscopy were prepared by direct mixing of equimolar amounts of two complementary single strands in phosphate-buffered saline (PBS, pH 7.5). The mixtures were then incubated at 95 °C for 10 min and afterward left to cool at 23 °C for 16 h. The equimolarity of the mixture and the integrity of the formed duplexes were checked by polyacrylamide gel electrophoresis (PAGE) electrophoresis. The resulting

~2 mM (in duplex) samples with a total ionic strength of 100 mM NaCl were also used for the Raman measurements.

Double helices for the STM measurements were chemically attached¹⁴ to self-assembled 40 nm thin monolayers of Au (99.99% purity). The monolayers were vacuum-evaporated on single crystalline silicon substrate (100) wafers, which were cut into 1 cm × 1 cm pieces, and the substrates were blown using pure nitrogen and exposed to a solution of thiolated oligonucleotides in a sodium chloride buffer. Five microliters of the 50 μM solution of 5'-thiol-modified single-stranded oligonucleotides was spotted onto the gold support, forming a drop of approximately 3 mm in diameter. The spotted slides were kept closed in a cartridge with a humidified atmosphere created by water-filled basins. The cartridge was incubated at 50 °C for 16 h, after which the gold support was washed twice with Milli-Q water. The spots were then treated with 5 μL of 1 mM 2-mercaptoethanol (2-ME). 2-ME was used to enhance the accessibility of the immobilized single strands to their complementary sequences because 2-ME thiol groups rapidly displace the weaker absorptive contacts between the nucleotides and the gold support, leaving the single strands tethered primarily through their thiol end groups. The single strands in the spots are "self-aligned", because the gold support is hydrophobic and any water present on its surface concentrates in the oligonucleotide-containing spots. The slides were incubated in the same humidified cartridge at 40 °C for 2 h, after which the slides were washed five times with Milli-Q water and dried under nitrogen. The duplexes were prepared by hybridization of the immobilized single strands with their corresponding complementary oligonucleotides:¹⁴ The complementary strands (~1 μM) were incubated in a hybridization buffer (100 mM Tris-HCl/100 mM NaCl) at 80 °C for 10 min, and immediately after that, 5 μL of the solution was dropped onto the corresponding spots and incubated at 40 °C for 1 h. Subsequently, the spots were washed twice by a washing buffer (100 mM Tris-HCl/300 mM NaCl) and finally by Milli-Q water, and the slides were dried under a stream of nitrogen. The entire process was photographed for easier alignment of the STM tip onto the duplex spots.

2.2. Experimental Section. 2.2.1. STM. Historically, two basic experimental approaches have been pursued in investigating conduction through molecules: (i) contacting isolated single molecules or molecules in thin films and (ii) studying transport in thick films and devices. The optimal experimental setup is to position isolated molecules between two electrical contacts, but this is very difficult to implement and especially difficult to verify. Working with the ordered arrays of parallel π -conjugated molecules, where in principle the binding to the substrate

can be precisely controlled, offers an opportunity to measure the individual molecules by making use of a STM tip.^{34–36} STM has also been used to investigate room temperature electronic properties of dodecamer d(GC)₁₂ attached to the gold surface by a thiol link.³⁷

We used the STM technique to study charge transport at ambient conditions through these types of oligonucleotides: canonical (STANDARD), canonical with majority of CG pairs (STANDARD CG), mismatched (MSMCH3), and abasic (ABASIC3, ABASIC4, and ABASIC5) nucleotides (Table 1). The STM measurements were performed with the NTEGRA Prima NT MDT system. Both topographic and spectroscopic data were obtained using freshly cut Pt/Ir tips. Using STM, the topography of the samples was observed for a set point of low voltage of ~10 mV and a relatively high current of ~0.5 nA and, therefore, at quite a small tip–sample distance. The topographic images showed a considerable difference between the bare gold substrates and the samples with DNA molecules. In the case of molecular layers, specific surface patterns were observed. The occurrence of these patterns was attributed to the corrosion of the bottom gold layers arising from the reaction of the thiol groups with the gold atoms, forming dissolvable complexes.^{34,38} The orientation of DNA molecules at the gold surface was investigated by variable angle spectroscopic ellipsometry (VASE, J. A. Woollam & Co.) working in the rotating analyzer mode. The measurements were carried out in a spectral range between 300 and 100 nm at three angles of incidence, namely, 65, 70, and 75°. We constructed a structural model consisting of Si substrate/Au layer/DNA layer. The Si substrate was considered as a semi-infinite medium; the optical constants of the Si and Au materials were taken from literature.³⁹ The thicknesses of both layers and the optical constants of the DNA layer were determined using a direct fitting procedure applied to the experimental ellipsometric data. The DNA molecules were ordered in similar geometric structures with the nearest-neighbor spacing being 1–2 nm. The thickness of the DNA layers determined by ellipsometry was 8.5–9.0 nm. For 32-nucleotide-long DNA molecules, this length corresponds to the average distance between the neighboring bases of about 0.3 nm, which in turn corresponds to the base–base stacking distance intermediate between the B- and the A-DNA forms. The DNA double helix is not likely to be completely straight; its deviation from the vertical line for 32 base pairs is expected to be about 25° for a persistent length *P* of 150 base pairs. We therefore conclude that DNA molecules are highly likely oriented approximately perpendicularly to the Au substrate.

STM experiments were carried out for pairs of samples on one chip, and all 15 combinations of two different oligonucleotides were measured so that each of the studied duplex was compared with all of the others. The tip–sample distance was controlled by combining two experimental setups. First, we worked in the constant height mode on a very small area on both sides of the compared oligonucleotide type border. Second, beside the current–voltage [*I(V)*] characteristics, we also measured *I(h)* curves (where *I* is the current and *h* is the distance between the tip and the surface) at the same points. *I(h)* curves have the advantage of being normalized and allow the reading of a sequence of a DNA molecule via tunnel–current decay.⁴⁰ The *I(h)* decay consists of two regions: an area of very short-range chemical interactions between the end of the tip and the termination of the molecule plus an area of tunneling through the barrier between the tip and the sample. The current initially decays slowly and then more rapidly; the *I(h)* curves are normally fitted with two exponentials:

$$i = i_0 \exp(-\beta_1 h), \quad 0 < h < h_c$$

$$i = i(h_c) \exp[-\beta_2(h - h_c)], \quad h_c < h$$

The value of β_2 was found in the literature^{22,39,40} as corresponding to the decay constant of the tunneling current. It can therefore be assumed that the interactions with the tip extremely close to the substrate are broken and the tunnel current becomes dominant at the breakpoint, h_c . The same position of the breakpoint and the same values of decay constants (β_2 and β_1) indicate the same tip–surface interaction conditions, so that working with different set points, we were able to position the tip in the proper interaction territory and the distance between the tip and the DNA termination was under control. We controlled the position of the tip above the samples by comparing the histograms of the decay constants and the breakpoints (h_c) of the *I(h)* curves measured for various DNA samples.

We measured the current passing through the molecules so close to the tip that their contribution at the set voltage was higher than the noise. When the tip is very close to the molecules (defined by the set point value) at very low voltages, the number of the molecules contributing to the total current is low. The current–voltage characteristics were recorded for various feedback voltage and current set points, that is, for different initial sample–tip distances. In all experiments, the STM tip acted as the electrical contact on the “top” side of the assembled monolayer of the DNA molecules, whereas the supporting gold substrate acted as the other “bottom” contact. The distance between the top of the molecules and the STM tip for all of the set points was estimated as 2.5–4 Å.

The *I(V)* and *I(h)* curves were measured at three different set points, 0.1 nA and 0.1 V, 0.2 nA and 0.1 V, and 0.5 nA and 0.1 V, and three different sample–tip separations for all samples. The experimental conditions were controlled using the *I(h)* decay analysis, which enabled us to distinguish between the area of tunneling current and the current passing through chemically interacting systems. The experimental setup (tip very close to the surface) allows us to expect that the current flows mainly through the molecule nearest to the tip without significant lateral intermolecular contribution to conduction. Two hundred consecutive *I(V)* sweeps in both voltage directions were taken for each sample, and the presented results are based on the average of a set from the collected *I(V)* curves. Only those curves that were not affected significantly by the drift of the STM were included in the statistics.

2.2.2. Raman Spectroscopy. To relate the intrachain conductivity of the DNA duplexes to the structural and conformational perturbations caused by the presence of mismatched base pairs and extensive abasic lesions, the Raman spectra of the canonical (STANDARD and STANDARD GC) and modified (MSMCH3, ABASIC4, and ABASIC5; Table 1) duplexes were studied in aqueous solutions at varying temperatures. Nonresonance Raman spectroscopy was applied, because Raman spectra without resonance enhancement of the aromatic bases also exhibit bands sensitive to the stacking and pairing of the bases, as well as conformationally sensitive Raman bands of the sugar phosphate backbone.

Raman spectra were excited with the 532 nm line of a continuous-wave solid-state Nd:YVO4 laser (Verdi 2, Coherent) using 200–300 mW of power at the sample. The spectra were collected in the 90 °C scattering geometry using a multichannel Raman spectrograph (Jobin Yvon-Spex 270 M) equipped with

a holographic notch-plus filter (Kaiser) to reject Rayleigh scattering and a liquid nitrogen-cooled CCD detector (Princeton Instruments). The measurements were carried out in a stationary temperature-controlled quartz microcell (5 μL of volume). The spectra were taken as a function of the temperature in a range of 2–98 $^{\circ}\text{C}$, with a temperature step of 3–10 $^{\circ}\text{C}$. Before taking a spectrum, the temperature of the sample was stabilized for 5 min, and reversibility of the temperature-induced changes was tested at several temperatures. Raman spectra for a given temperature were recorded as six consecutive 100 s long accumulations. In such a way, it was possible to distinguish potential spectral changes because of laser illumination from the changes induced by a temperature increase. Wavenumber scales of the Raman spectra were precisely calibrated using the emission spectra of a neon glow lamp taken before and after each Raman measurement. The Raman contribution from the buffer was carefully subtracted, and the spectra were corrected for their background using advanced methods of factor analysis. Afterward, all of the spectra were normalized to the peak height of the 1093 cm^{-1} band associated with the PO_2^- symmetric stretching mode, reported previously to be largely invariant to the melting of DNA duplexes.⁴¹

2.3. Computer Modeling. 2.3.1. MD Simulations. Three double-stranded 32-mer long oligonucleotides were studied as follows: the canonical STANDARD, MSMCH3 with three mismatched base pairs, and ABASIC3 with three central pairs of nitrogenous bases replaced by methyl groups. MD simulations were carried out with the AMBER program, version 8, with the parmbsc0 force field.^{42,43} The charge of DNA molecules was compensated by Na^+ cations, and all of the three duplexes were embedded in a box of dimensions 47 $\text{\AA} \times 47 \text{\AA} \times 133 \text{\AA}$ filled with TIP3P water molecules. The simulations started for molecular models with the sugar phosphate backbone in the fiber conformation as furnished by the AMBER program. Prior to the MD simulations, a six-step equilibration was carried out when the solvent geometry was relaxed and the DNA geometry kept rigid, after which both solvent and DNA geometries were relaxed, and finally, a heating/equilibration simulation was performed at a constant volume with rigid DNA and temperature increased from 0 to 300 K. The actual MD simulation was run for 10 ns using the periodic boundary conditions at a temperature of 300 K and a cutoff at 10 \AA .

2.3.2. DFT Quantum Mechanics Calculations. Molecular models for quantum mechanics calculations included only the central part of the DNA duplexes that the MD simulations had shown to be the most flexible. Three models were built based on the STANDARD, MSMCH3, and ABASIC3 oligonucleotide, respectively: The STANDARD' duplex consisted of five base pairs [5'-d(TCGGA)-3'•5'-d(AGCCT)-3']; the ABASIC3' model contained 5'-d(TXXXA)-3'•5'-d(AXXXT)-3' with two flanking A-T pairs and three base pairs substituted by methyl groups in the center; the MSMCH3' model contained three mismatches in the duplex [5'-d(TCCGA)-3'•5'-d(ACCTT)-3']. Electronic characteristics of each molecular model were calculated for six coordinate sets that were extracted from the MD simulations at 0, 1, 2, 3, 4, and 5 ns. To examine the electronic structure of DNA under various structural and solvation conditions, each coordinate set of each model was considered at three levels of solvation: Nonhydrated ("isolated") system and two systems containing 50 and 110 water molecules, respectively. All DFT calculations were performed directly using the molecular geometries from the MD calculations as single-point calculations without any further structure optimization. The positions of the Na^+ counterions were fixed relative to the PO_4^- groups: The

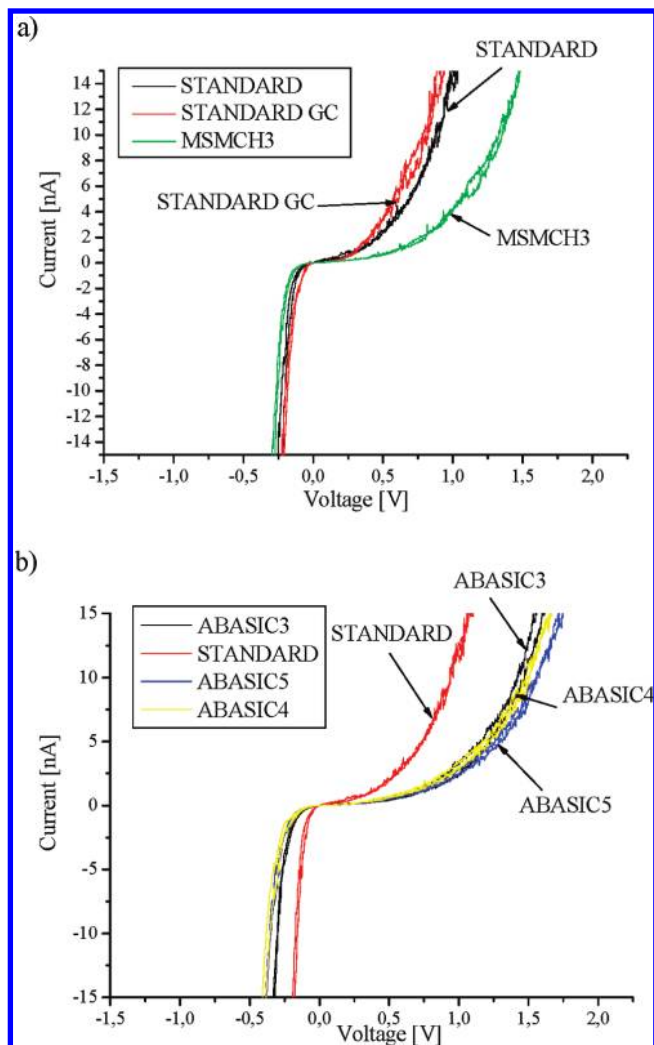


Figure 1. Typical STM $I(V)$ curves of DNA 32-mer oligonucleotide double strands. (a) STANDARD (black), STANDARD GC (red), and MSMCH3 (green). (b) ABASIC3 (black), ABASIC4 (yellow), ABASIC5 (blue), and STANDARD (red). The STM set points were 0.1 nA and 0.1 V, and the $I(V)$ curves were measured in both voltage directions.

$\text{Na}^+\cdots\text{P}$ distances were kept at 2.22 \AA , a value obtained from the geometry optimization of the single-stranded pentanucleotide. The test calculations with the STANDARD' model showed a decrease of the highest occupied molecular orbital (HOMO)–lowest unoccupied molecular orbital (LUMO) gap with an increase of the $\text{Na}^+\cdots\text{P}$ distances, and for distances larger than 5.0 \AA , the calculations did not converge.

The quantum chemical calculations were performed using the Gaussian 03 software package.⁴⁴ The 6-31G* polarized double- ζ basis sets together with M05-2x functional⁴⁵ designed for the study of weak interactions and π – π interacting systems were used in the density functional theory (DFT) calculations.

3. Results

3.1. STM. Using the STM technique, we found that the conductivity of the duplexes decreases with the extent of their structural perturbations in the following order: STANDARD CG > STANDARD \gg MSMCH3 > ABASIC3 > ABASIC4 > ABASIC5 (Figure 1).

Both canonical duplexes are expected to be structurally similar and the most ordered of all samples; their conductivity does not differ significantly. A relative change of conductivity

between two samples measured on one chip was estimated as the ratio of their currents measured at 1 V. This ratio between STANDARD CG and STANDARD is 1.2, indicating no significant difference. The introduction of three mismatched base pairs resulted in a pronounced conductivity decrease as compared to STANDARD: The conductivity ratio STANDARD/MSMCH3 was about 2.7. Elimination of three, four, and five base pairs in the ABASIC3, ABASIC4, and ABASIC5 sample, respectively, resulted in a large conductivity decrease as compared to STANDARD: The conductivity ratio between STANDARD and ABASIC3 was 3.3, a further drop in charge transfer with more base pairs removed is however slower (ABASIC3/ABASIC5, 1.3). The conductivity decrease from MSMCH3 to ABASIC3 is perhaps surprisingly small (MSMCH3/ABASIC3, 1.2); the difference is shortly discussed in the light of structural results by Raman, MD, and DFT approaches below.

The applied potential eV drops entirely between the tip of the STM probe and the DNA molecule, whereas the molecular electrochemical potential remains fixed with respect to the gold substrate (assuming a sufficiently small capacitance of the interface between the table electrode and the DNA). For a positive substrate voltage, the molecule starts to conduct when the electrochemical potential of the tip reaches the level of the LUMO; for negative substrate voltage, the molecule conducts as the potential of the tip approaches the HOMO. Therefore, the $I(V)$ characteristics are expected to be asymmetric for molecules coupled to the gold surface by the thiol link since the HOMO is a sulfur-based level that couples strongly to gold, whereas the LUMO couples only weakly and the current should be smaller for positive substrate voltage (LUMO conduction) than for negative substrate voltage (HOMO conduction). It should be emphasized that this asymmetry is not present if there is a shift in the molecular energy levels under applied bias.¹⁴

The STM method using the setup with one end of DNA connected by a chemical bond to the conductive gold surface and with an air gap between the other end of the DNA molecule and the metallic tip provides an alternative way to determine the polarity of the prevailing charge carriers. The voltage in the Ntegra Prima setting is applied to the table, and the electric current (conventional direction) flows from the table to the tip. Provided that standard models of nanodevices⁴⁷ are applied and the contact capacitances are neglected, the chemical potential of the measured DNA samples is much closer to the top of the valence-state energy band (HOMO) than to the bottom of the conduction band-state energies (LUMO), which corresponds to a material with prevalently p type (hole) electric conductivity.⁴⁸

3.2. Raman Spectroscopy. Normalized Raman spectra (Figure S1 of the Supporting Information) of five studied duplexes (STANDARD, STANDARD GC, MSMCH3, ABASIC4, and ABASIC5) exhibit features typical of the thermal disordering of double-stranded nucleic acids.⁴⁶ The final disorder reached at 98 °C evidently converges for all of the duplexes, but low-temperature regularities and details of their melting profiles do differ between samples. Using more detailed analyses, noticeable differences between the canonical, the mismatched, and the abasic duplexes can be found in the melting profiles of their prominent Raman bands, as shown in Figure 2 and in the Supporting Information.

The structural perturbations at the level of the base pair arrangement can be monitored via bands assigned to the vibrations of the purine and pyrimidine bases that undergo a significant increase of intensity and/or frequency shifts as the bases become unstacked and/or unpaired.^{41,46} As an example of temperature-induced Raman changes, the melting curve of

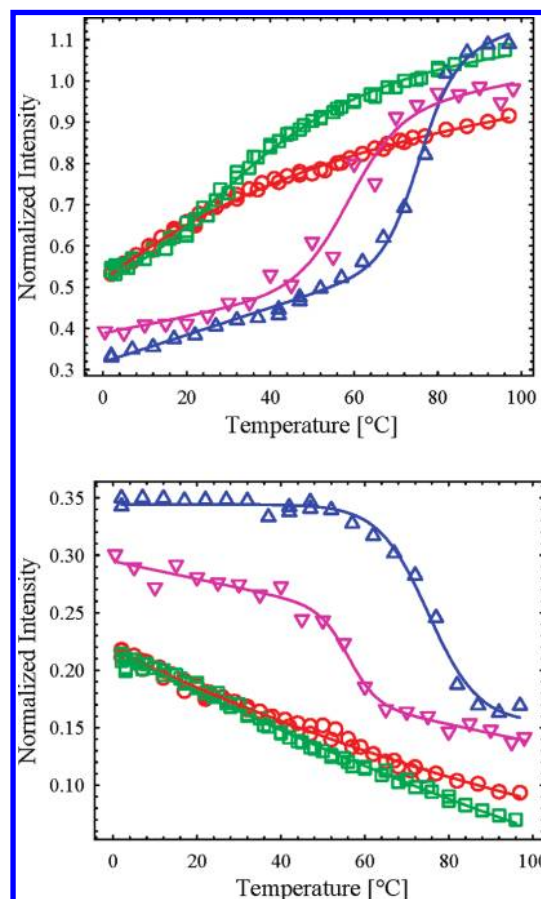


Figure 2. Melting profiles of the representative Raman bands from the normalized spectra of STANDARD (blue triangles facing up), MSMCH3 (pink triangles facing down), ABASIC4 (red circles), and ABASIC5 (green squares). Normalized intensities of the thymine band at 1238 cm^{-1} (left) and the phosphodiester band at 834 cm^{-1} (right) are shown as a function of temperature.

the thymine band at 1238 cm^{-1} sensitive to unstacking and/or unpairing is shown in Figure 2. The linear increase of the intensity at 1238 cm^{-1} observed for the canonical duplexes below 45 °C is considered to be a typical Raman signature of the DNA premelting phase, when the regular double helix is structurally altered but not dissociated into single strands. The spectral changes reflecting cooperative transition in a temperature interval of $70\text{--}80\text{ °C}$ ($T_m = 76 \pm 1\text{ °C}$) are followed by subsequent postmelting temperature-dependent structural alterations of the base arrangement within the separated single strands. The cooperative melting profile is thus superimposed on the premelting/postmelting linear background (Figure 2). In the case of the canonical and mismatched duplexes, a similar behavior was observed for the majority of the bands assigned to the vibrations of the bases, providing mean median melting temperatures of 76 ± 2 and $56 \pm 2\text{ °C}$, respectively. The spectral characteristics of the purine and pyrimidine bands in both abasic DNAs seem to be changed much more gradually with hardly perceptible (ABASIC5, $T_m = 33 \pm 3\text{ °C}$), if any (ABASIC4), cooperativity.

Although the height of the band at 1093 cm^{-1} was postulated to be temperature insensitive⁴⁶ and was therefore used as an internal intensity standard also in the present study, its half-width (fwhm) was found to increase with temperature (Figure S2 of the Supporting Information). The same broadening reported previously upon the melting of various DNA duplexes was attributed to changes in the PO_2^- environment,⁴⁶ likely due

to altered interactions with water and metal ions. Taking the fwhm of the 1093 cm^{-1} band as a quantitative measure, the average environment experienced by the phosphate groups in the abasic duplexes at $2\text{ }^{\circ}\text{C}$ resembles that in the considerably disordered canonical or mismatched oligomers (Figure S2 of the Supporting Information). Like the melting profiles of the bands indicating changes of base stacking and pairing discussed above, the cooperative character of the PO_2^- melting profiles of the STANDARD ($T_m = 77 \pm 1\text{ }^{\circ}\text{C}$, $\Delta\text{fwhm} = 5.5\text{ cm}^{-1}$) and mismatched (MSMCH3, $T_m = 58 \pm 1\text{ }^{\circ}\text{C}$, $\Delta\text{fwhm} = 4.7\text{ cm}^{-1}$) duplexes contrast with gradual thermal denaturation of the abasic DNAs that shows hardly perceptible (ABASIC5, $T_m = 35 \pm 3\text{ }^{\circ}\text{C}$, $\Delta\text{fwhm} = 2.2\text{ cm}^{-1}$), and virtually no (ABASIC4, $\Delta\text{fwhm} = 3.1\text{ cm}^{-1}$), cooperativity.

The gradual elimination of the regular B-DNA structure with increasing temperature can also be monitored by the intensity decrease of the Raman band at 834 cm^{-1} (Figure S1 of the Supporting Information), assigned to the phosphodiester ($\text{C3}'\text{-O-P-O-C5}'$) stretching, diagnostic of the geometry typical of B-DNA.⁴⁶ As the population of the B-ordered phosphodiester groups decreases with increasing temperature, the 834 cm^{-1} band is replaced by a broad and weak distribution of Raman intensity extending from 800 to 850 cm^{-1} .⁴⁶ This band is considerably weaker and broader in the abasic duplexes even at $2\text{ }^{\circ}\text{C}$, which signifies greater conformational heterogeneity of their phosphodiester backbones than the heterogeneity of the canonical or mismatched duplexes at temperatures as high as $50\text{ }^{\circ}\text{C}$. Even though sugar phosphate backbones of the abasic duplexes are partially disordered even at the lowest temperatures, they still belong to the B-DNA conformational family.

The Raman experiments showed that the absence of a few consecutive base pairs in the middle of duplexes (ABASIC4 and ABASIC5) represents a considerably greater structural disturbance than the presence of mismatched base pairs, and the missing base pairs have a much more pronounced effect on the overall duplex structure than the base pair mismatches. Using the melting profiles of the bands of DNA nucleotides and those of the sugar phosphates separately as a measure of the relative irregularity with respect to canonical DNA, the base pair arrangement of both abasic oligomers at low temperatures seems to be more preserved than the regularity of their sugar phosphate backbones. The regularity of the low-temperature state ($2\text{ }^{\circ}\text{C}$) of abasic DNAs considered in terms of nucleotide vibrations corresponds to the end of premelting phase of the canonical duplex, whereas the characteristics of the sugar phosphate backbone suggest a more progressed disorder approaching the level of the melting/postmelting phase. This finding may reflect the persistence of base pairing and base stacking within the intact parts of the abasic duplexes despite a considerable irregularity of their sugar phosphate backbones. Alternatively, the phosphates from the abasic part may be exposed to a different environment than phosphates in the parts with bases, shifting the mean spectral features toward a seemingly more disordered structure.

3.3. Computer Modeling. **3.3.1. MD.** MD calculations were carried out to model global structural changes and dynamical behavior of the DNA duplexes with mismatches (MSMCH3) or missing base pairs (ABASIC3) and to compare the results with global topology and flexibility of the canonical B-DNA (STANDARD). The MD simulations of all three models started from the same fiber DNA, but their conformations began to differ within the first 2 ns: The root mean square deviations (rmsd) related to the initial structure reached the values around 4 \AA for STANDARD and MSMCH3, while they were around

9 \AA for the ABASIC3 (Figure S3 of the Supporting Information). The global structural change of the ABASIC3 molecule is significant, and its structural behavior differs from the canonical and mismatched DNA structures because the three missing base pairs in the central part of the duplex destabilize the duplex and increase its flexibility up to a point where the two strands approach each other at the site of the structural perturbation (Figure S3 of the Supporting Information). In contrast, global structural perturbations in MSMCH3 measured by the rmsd statistics are small, but the local structural changes near the three mismatched base pairs are quite large, as shown below.

The local changes occurring at the site of the structural perturbations—three mismatches in MSMCH3 and three missing base pairs in ABASIC3—were estimated by calculating the distances between the $\text{C1}'$ atoms of the facing sugar rings at the opposite strands (Figure 3; $\text{C1}'$ is a carbon atom belonging to the sugar ring making a link to the nucleobase). The distances in the STANDARD model fluctuated in a very confined interval around 11 \AA , indicating a compact and regular structure along the whole 10 ns trajectory. In MSMCH3, the distances are also fairly stable, but their values are different for different mismatches. Of the three mismatched pairs, only G-T is isometric with the W-C pairs, and its $\text{C1}'\text{-C1}'$ distance is indeed near 11 \AA like in STANDARD. The other two mismatches are formed by C-C pairs and have smaller $\text{C1}'\text{-C1}'$ distances, about 7 \AA . The ABASIC3 model behaves differently from the previous two; the $\text{C1}'\text{-C1}'$ distances between the missing bases vary from 5 to 25 \AA , and their wild fluctuations (they doubled in the second part of the MD trajectory) indicate disorder of the central part of the model. Large structural fluctuations in the noncanonical segment of ABASIC3 indicate local instability that presents itself by formation of a sharp and variable kink between the two terminal W-C-paired segments (Figure S3 of the Supporting Information). It should be, however, noted that these two terminal segments sustain a relatively stable double-helical structure. The fluctuations cause shortening of the effective length of the ABASIC3 molecule as compared to STANDARD or MSMCH3.

Despite the regular double-helical nature at both ends of ABASIC3, the disordered central part disrupts the long-range regularity of the structure in its base stacking but also in the backbone part. The regularity and stability of MSMCH3 are diminished to a much smaller but measurable extent when compared to the STANDARD sample and is less regular and more flexible.

3.3.2. DFT Calculations. DFT quantum mechanics calculations were performed in a time evolution as had been modeled by the MD simulations to highlight the electronic and structural factors that may impact the charge carrier transport in the studied molecules. Table 2 and the Supporting Information (Tables S1–S6) summarize the orbital energies and the character of the frontier orbitals for the isolated and hydrated models (the geometries correspond to the MD snapshots at 0 and 5 ns). Table 3 shows that the presence of water molecules decreases the averaged HOMO–LUMO gaps for all of the models. The LUMOs are localized at the Na^+ counterion in all of the cases examined. The highest lying molecular orbitals HOMO and HOMO-1 (molecular orbitals lying nearest to HOMO in the energetic scale) for all of the systems with 50 water molecules are depicted in Figure S4 of the Supporting Information.

Results of the previous works on single- and double-stranded DNA^{4,7,47–49} have pointed to the hole conductivity occurring through the set of highest occupied orbitals. The electron transfer

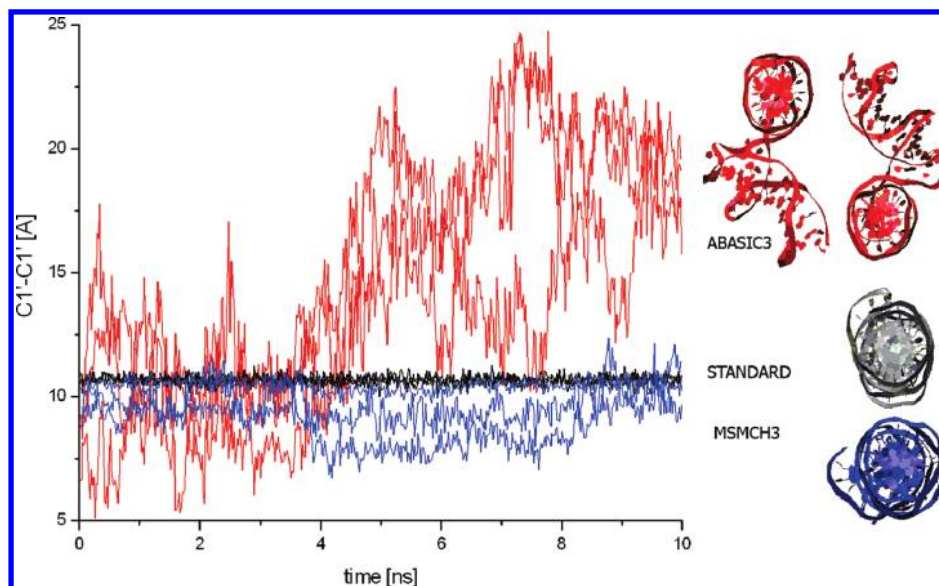


Figure 3. Distances calculated between the carbons C1' of deoxyriboses 15 and 17 as a function of the simulation time for STANDARD (black), MSMCH3 with the mismatched pairs (blue), and ABASIC3 with three abasic nucleotides (red). The projections on the right side show views along the molecular axis after 10 ns of MD simulations. The ABASIC3 molecule is shown twice from the “top” and “bottom” to emphasize that both of its ends are well-preserved B type double helices and that only the central region is highly disordered.

TABLE 2: Orbital Energies of the Frontier Orbitals and Their Main Contributions for the STANDARD', MSMCH3', and ABASIC3' Models Solvated by 110 Water Molecules at the MD Simulation Time of 5 ns

orbitals	energy (eV)	main component of the orbital
STANDARD		
LUMO	-0.93	Na + PO ₄ ⁻ (weak) + water (weak)
HOMO	-6.31	guanine + water (very weak)
HOMO-1	-6.53	guanine
MSMCH3		
LUMO	-1.11	Na + PO ₄ ⁻ (weak) + water (weak)
HOMO	-4.79	guanine + cytosine (weak)
HOMO-1	-5.42	cytosine + sugar (very weak)
ABASIC3		
LUMO	-1.29	Na + PO ₄ ⁻ (weak) + water (weak)
HOMO	-6.56	water
HOMO-1	-6.65	water

TABLE 3: Differences between Energies of the Frontier Orbitals HOMO, HOMO-1, and LUMO Averaged over the Modeled MD Simulation Times of 0, 1, 2, 3, 4, and 5 ns

model	HOMO–LUMO (eV)	HOMO–HOMO-1 (eV)
STANDARD		
nonhydrated	3.92	0.21
110 water molecules	3.61	0.19
MSMCH3		
nonhydrated	3.64	0.31
110 water molecules	2.68	0.31
ABASIC3		
nonhydrated	5.66	0.18
110 water molecules	4.71	0.38

integral that indicates the measure of charge transport probability can be estimated as one-half of the HOMO and HOMO-1 orbital energies.^{48,50} Values of the integral suggest that the charge transfer is likely through HOMO orbitals localized on the DNA bases in STANDARD' and MSMCH3' (Supporting Information, Figure 4). Water molecules increase the charge transport probability because their π -orbitals contribute to the high-energy orbitals, including HOMO. The HOMO and HOMO-1 orbitals of the isolated (nonhydrated) STANDARD' and MSMCH3' are formed by guanine and cytosine π -orbitals but in systems

containing water are contributed or formed by water orbitals (see Tables S1–S4 in the Supporting Information). The time-averaged HOMO–HOMO-1 gap of the STANDARD' molecule was smaller (0.19 eV) than that of the MSMCH3' system (0.31 eV, Table 3), and the HOMO orbitals of MSMCH3' were less uniformly spread in real space than those of STANDARD'. Both facts relate to a lower probability of charge transport with possible creation of traps on mismatched chains.

The situation differs in the ABASIC3' model. Molecular orbitals localized on water molecules contribute to the ABASIC3' conductivity even at 0 ns because of a small difference between the energies of the orbitals at the bases and water; they can therefore more effectively mediate the charge transfer (Figure S5 of the Supporting Information). The time-averaged separation between HOMO and HOMO-1 in ABASIC3' varies with different levels of hydration more than for MSMCH3' and STANDARD'. Geometries at longer times of the MD simulations have lower energies of the adenine-based molecular orbitals (Tables S5 and S6 of the Supporting Information), and the HOMOs are formed by localized water states. As the distances between the bases in ABASIC3' enlarge with time of the MD simulations from 11.5 Å at 0 ns to 16.4 Å at 5 ns, water orbitals represent the only possible pathway for charge transport. The role of the solvent on the structure relaxation is in the case of abasic DNA very large: After 5 ns, the change of physical structure estimated by MD and electronic structure estimated by DFT in the solvent is by far the largest of all investigated models.

Results of the DFT calculations can be summarized for the STANDARD' and MSMCH3' models as follows:

- The charge transfer via HOMO orbitals is localized on the DNA bases, and water molecules increase the charge transport probability.
- HOMO orbitals are less uniformly distributed in space in mismatched than in W-C models.
- Both solvation models of STANDARD' have a smaller time-averaged HOMO–HOMO-1 energy gap and a higher probability for the complex type of charge transport than the MSMCH3' models.

For the ABASIC3' models:

- The charge transport probability is the lowest of all of the three solvation models mainly due to the low interaction of orbitals localized at distant bases.
- The time-averaged HOMO–HOMO-1 separation is larger than in STANDARD' and MSMCH3' and changes with hydration levels.
- Water molecules either contribute to or even form the HOMO orbitals and consequently strongly influence the charge transport across the abasic lesion, making a bridge between the noninteracting bases.

4. Discussion

The position of DNA among the biological and man-made polymers is quite unique due to its ability to preserve, transfer, and transmit information. All of these functions depend on the ability of the DNA molecule to self-assemble by forming an antiparallel double helix stitched by W-C pairs of complementary bases. Results of recent research have suggested that changes in charge transfer properties may serve as an indicator of DNA damage or even be used to repair some of its lesions.^{10,17–21,23} Moreover, if charge transport through DNA is fully understood, it may be of great interest for applications in the area of nanotechnology.

Two extreme mechanisms of charge transport in DNA can be considered. The prevailing DNA architecture, antiparallel double helix, has well-stacked bases with overlapping π -electron systems, and it is widely assumed that nearly parallel bases with overlapping π -electrons have highly delocalized molecular orbitals that are good candidates for long-distance, one-dimensional (linear) charge transport.⁸ The second possible charge transport mechanism in DNA is charge hopping that presumes localized molecular orbitals and no significant electronic overlap between adjacent base pairs. Unlike π -electrons that can form extended molecular orbitals, the DNA backbone, water molecules, and counterions in the solvation shell create localized states resulting in charge conduction by the phonon-assisted (thermally activated) hopping.^{11,13,51–54} There is one phenomenon that is important for charge transport in organic molecules: a polaron. A polaron is a radical charge self-trapped by a structural distortion of its containing medium.^{12,13,55} A polaron may migrate by tunneling or by phonon-assisted (thermally activated) hopping.⁵⁶ Electronic overlap between bases within the polaron is larger, because it is formed in response to a need for electron donation. As a consequence, the charge becomes delocalized within the base pairs in a polaron-like distortion, and its transport therein might appear to occur by a superexchange mechanism.⁵⁷ Structural fluctuations of base pairs transferred to their π -stack interactions have experimentally been shown to influence charge transfer of DNA duplexes.⁵⁸

Regardless of its exact mechanism, charge transfer through DNA duplex strongly depends on base composition. Preferential trapping of charge in the isolated guanine base,¹⁷ or more markedly at the GG steps, has been confirmed by several works. One-electron oxidation was mostly observed at the GG steps in the mixed GG/A/T sequences²⁵ with a proposed charge transfer mechanism by phonon-assisted polaron hopping. Quantum mechanical calculations confirmed by experimental findings^{28,59} indicate that one-electron oxidation of the 5'-guanine from the GG step is modulated by the flanking sequence due to steric effects.

Introduction of mismatches, non-W-C base pairs, to a DNA duplex changes its electrical properties. Signals from redox intercalators embedded in duplexes immobilized on gold

surfaces have shown marked sensitivity to the presence of base mismatches.²⁹ Mismatch detection was accomplished irrespective of DNA sequence and mismatch identity. Individual mismatches have also been identified by single-molecule fluorescence spectroscopy in solution⁶⁰ as a function of the DNA sequences. Single-particle measurements of electrical conductivity on DNA duplexes³⁰ have shown a large decrease of conductivity for duplexes with mismatched pairs, and lower charge transport and its distinct kinetic parameters can even be used to identify the kind of mismatch.⁶¹ All of these observations demonstrate that charge transfer characteristics of DNA duplex are able to reveal the presence of mismatches in the sequence, which may help elucidate possible mechanisms of mismatch identification in the cell as well as for mismatch identification in technological applications.

We used experimental and theoretical methods to study relationships between conductivity (STM), structure, thermal stability (Raman spectroscopy and MD), and the influence of the solvent water (DFT) in standard and modified DNA molecules to improve the understanding of the very complicated phenomenon of charge transport through DNA. Comparison of W-C-paired natural oligonucleotides with oligonucleotides containing various perturbations and mismatched and missing base pairs showed unexpected and interesting effects that extend the picture of the charge transfer mechanism through the DNA molecule.

The STM measurements presented here show a sequence-dependent manner of charge transfer through the duplex with GC-rich double strands having the largest conductivity. The STM data also show that any disruption of the canonical W-C base pairing or introduction of chemical modification to the DNA backbone or removal of base(s) leads to a lower conductivity; single-stranded DNA always has a lower conductivity than duplexes.^{14,62} A decrease of the conductivity in the sample MSMCH3 with three mismatched base pairs relative to STANDARD with all W-C pairs may seem large considering the preserved vertical π -stacking and overall stability of the MSMCH3; both properties are comparable in both samples as revealed by the analysis of Raman spectra and suggested by MD simulations. A possible explanation may be offered by the DFT calculations that show that the mismatched pairs constitute isolated electronic states requiring greater activation energy and their HOMO orbitals are less uniformly dispersed than regularly ordered W-C base pairs, further diminishing the charge transport probability. The abasic samples had still lower conductivity than the mismatched sample, but the decrease from MSMCH3 to ABASIC4 was moderate. It is perhaps surprising especially considering the complete removal of several base pairs that had dramatic consequences for the duplex stability and structural regularity, demonstrated clearly by the Raman experiments: While MSMCH3 with three non-W-C base pairs was only slightly less stable than the canonical duplexes and it melted in a cooperative way, the structural regularity and thermal stability of abasic duplexes were strongly affected.

One possible mechanism of charge transport in the abasic samples is by mixing DNA and solvent orbitals. The DFT calculations and MD simulations allow formulation of the hypothesis that water molecules entering the otherwise hydrophobic duplex interior at the abasic sites can partially compensate for the loss of overlap between the base orbitals and increase the conductivity. Considering substantial structural distortions around the abasic part of the duplexes, evidenced by Raman spectroscopy and supported by the MD simulations, charge transport solely through the base pairs would be highly

ineffective, if possible at all. Furthermore, albeit indirect, support for solvent-mediated charge transport comes from our DFT calculations that show mixing of the base and water HOMO orbitals. It is consistent with low temperature ($-78\text{ }^{\circ}\text{C}$) measurements of radiation-induced conductivity of W-C-paired DNA,¹⁵ providing strong evidence that charge transport is not mediated merely by overlapping π -orbitals of the bases in the core of the double-helical DNA but also by its outer mantle, that is, the sugar phosphate backbone and the first hydration shell. Further suggestion that hydration is of utmost importance for charge transport in DNA has been provided by calculations⁶³ of a lower potential barrier for the hole transfer between the hydrated rather than the “dry” W-C pairs. Moreover, the π -electron density redistribution activated by hydration is enhanced by the intrastrand interactions.

5. Conclusion

We combined various experimental and theoretical approaches (STM, Raman spectroscopy, MD, and DFT quantum mechanics) to study the relationships between the base pairing patterns and the charge transfer properties in DNA double-helical oligonucleotides. The STM measurements indicate that the best conductor is DNA in its biologically relevant double-stranded form with W-C base pairs: All modified duplexes, that is, DNA with mismatched (non-W-C) pairs and duplexes with abasic nucleotides, have a considerably lower conductivity. The STM-measured current–voltage characteristics point to a material with predominating hole type electric conductivity.

Analysis of conformationally and microenvironmentally sensitive Raman bands revealed that the structural regularity and thermal stability of duplexes decrease from the canonical W-C-paired double helix to the mismatched duplex and still significantly more to abasic duplexes. The MD simulations present the same picture with large conformational fluctuations of the sugar phosphate backbone at the abasic sites.

The DFT calculations show that water orbitals strongly influence charge transport for all of the models. For the W-C-paired and mismatched models alike, the HOMO orbitals are localized on the bases, and the water orbitals increase the charge transport probability. The lower conductivity and transport probability of the mismatched model can be explained by its less uniformly dispersed HOMO orbitals. The abasic samples had still lower conductivity than the mismatched sample, but the decrease from MSMCH3 to ABASIC4 was moderate. We assume that water is solely responsible for charge transport across the abasic lesion because only its orbitals can bridge the distant bases flanking the abasic site. Design of particular DNA sequences with chain or base modifications and/or noncanonical base pairing, enabling partial hydration of the interior of the duplexes, can be envisioned for future use of molecular wires of defined conductivity.

To summarize, comparison of natural W-C paired oligonucleotides with oligonucleotides containing perturbations caused by mismatched or missing base pairs showed unexpected and interesting effects. On the basis of our results, we can conclude that the charge transport depends not only on the base composition (and is mediated by overlapping π -orbitals of bases) but also on the DNA sugar phosphate backbone and the first hydration shell. Our theoretical studies explain the surprising experimental findings: (i) A decrease of the conductivity in the mismatch sample (as compared to standard DNA) was relatively large considering the preserved vertical π -stacking and overall stability, and (ii) the conductivity difference between mismatched and abasic samples was contrariwise surprisingly small

provided that the Raman experiments plus MD calculations showed that the absence of a few consecutive base pairs in the middle of duplexes represents a considerably greater structural disturbance than the presence of mismatched base pairs. We found that a potential barrier is lower for the hole transfer between the hydrated and the “dry” W-C pairs. In the case of mismatched pairs, isolated electronic states require greater activation energy and their HOMO orbitals are less uniformly dispersed than the regularly ordered W-C base pairs.

Acknowledgment. This work was supported by the Academy of Sciences of the Czech Republic Grants Nos. IAA400550701, KAN401770651, KAN200100801, and KAN100400702; the Czech Science Foundation 203/08/1594, 202/07/0643, and 202/09/0193; the Ministry of Education of the Czech Republic (MSM0021620835); and institutional funds of the Institute of Physics AS CR, vvi (AV0Z10100520) and the Institute of Biotechnology AS CR, vvi (AV0Z50520701). The computer time at the MetaCentrum Brno is gratefully acknowledged.

Supporting Information Available: Figures of the representative Raman spectra; melting profiles of the representative Raman bands from the normalized spectra; rmsd of the geometries along the trajectory in dependence on the simulation time calculated for the DNA samples; schematic representation of HOMO and HOMO-1; and schematic representation of the four upper-lying HOMOs; and tables of orbital energies and main contributions to the frontier orbitals. This material is available free of charge via the Internet at <http://pubs.acs.org>.

References and Notes

- Holmlin, R. E.; Dandliker, P. J.; Barton, J. K. *Angew. Chem., Int. Ed. Engl.* **1997**, *36*, 2715.
- Nunez, M. E.; Hall, D. B.; Barton, J. K. *Chem. Biol.* **1999**, *6*, 85.
- Odom, D. T.; Dill, E. A.; Barton, J. K. *Chem. Biol.* **2000**, *7*, 475.
- Schuster, G. B. *Acc. Chem. Res.* **2000**, *33*, 253.
- Giese, B. *Acc. Chem. Res.* **2000**, *33*, 631.
- Troisi, A.; Orlandi, G. *Chem. Phys. Lett.* **2001**, *344*, 509.
- Starikov, E. B.; Tanaka, S.; Kurita, N.; Sengoku, Y.; Natsume, T.; Wenzel, W. *Eur. Phys. J. E* **2005**, *18*, 437.
- Cohen, H.; Nogues, C.; Naaman, R.; Porath, D. *Proc. Natl. Acad. Sci. U.S.A.* **2005**, *102*, 11589.
- Taniguchi, M.; Kawai, T. *Phys. E* **2006**, *33*, 1.
- Wagenknecht, H. A. *Nat. Prod. Rep.* **2006**, *23*, 973.
- Qian, J.; Liao, S. C.; Xu, S.; Stroschio, M. A.; Dutta, M. *J. Appl. Phys.* **2009**, *106*.
- Tran, P.; Alavi, B.; Gruner, G. *Phys. Rev. Lett.* **2000**, *85*, 1564.
- Endres, R. G.; Cox, D. L.; Singh, R. R. P. *Rev. Mod. Phys.* **2004**, *76*, 195.
- Kratochvílová, I.; Kral, K.; Buncek, M.; Visková, A.; Nespurek, S.; Kochalska, A.; Todorciuc, T.; Weiter, M.; Schneider, B. *Biophys. Chem.* **2008**, *138*, 3.
- Warman, J. M.; deHaas, M. P.; Rupprecht, A. *Chem. Phys. Lett.* **1996**, *249*, 319.
- Conwell, E. M.; Bloch, S. M.; McLaughlin, P. M.; Basko, D. M. *J. Am. Chem. Soc.* **2007**, *129*, 9175.
- Lewis, F. D.; Wu, T.; Zhang, Y.; Letsinger, R. L.; Greenfield, S. R.; Wasielewski, M. R. *Science* **1997**, *277*, 673.
- Wagenknecht, H. A.; Stemp, E. D. A.; Barton, J. K. *J. Am. Chem. Soc.* **2000**, *122*, 1.
- Heller, A. *Faraday Discuss.* **2000**, *1*.
- Friedberg, E. C. *Nature* **2003**, *421*, 436.
- Kanvah, S.; Schuster, G. B. *Nucleic Acids Res.* **2005**, *33*, 5133.
- Arkin, M. R.; Stemp, E. D.; Holmlin, R. E.; Barton, J. K.; Hormann, A.; Olson, E. J.; Barbara, P. F. *Science* **1996**, *273*, 475.
- Dandliker, P. J.; Holmlin, R. E.; Barton, J. K. *Science* **1997**, *275*, 1465.
- Shao, F. W.; Barton, J. K. *J. Am. Chem. Soc.* **2007**, *129*, 14733.
- Liu, C. S.; Schuster, G. B. *J. Am. Chem. Soc.* **2003**, *125*, 6098.
- Genereux, J. C.; Augustyn, K. E.; Davis, M. L.; Shao, F.; Barton, J. K. *J. Am. Chem. Soc.* **2008**, *130*, 15150.
- Grozema, F. C.; Tonzani, S.; Berlin, Y. A.; Schatz, G. C.; Siebbeles, L. D. A.; Ratner, M. A. *J. Am. Chem. Soc.* **2009**, *131*, 14204.
- Joseph, J.; Schuster, G. B. *J. Am. Chem. Soc.* **2009**, *131*, 13904.

- (29) Kelley, S. O.; Boon, E. M.; Barton, J. K.; Jackson, N. M.; Hill, M. G. *Nucleic Acids Res.* **1999**, *27*, 4830.
- (30) Guo, X. F.; Gorodetsky, A. A.; Hone, J.; Barton, J. K.; Nuckolls, C. *Nat. Nanotechnol.* **2008**, *3*, 163.
- (31) Beaucage, S. L.; Iyer, R. P. *Tetrahedron* **1992**, *48*, 2223.
- (32) Brown, D. M. A brief history of oligonucleotide synthesis. In *Protocols for Oligonucleotides and Analogs. Synthesis and Properties*; Agrawal, S., Ed.; Humana Press: Totowa, 1993; Vol. 20; p 1.
- (33) Reese, C. B. *Org. Biomol. Chem.* **2005**, *3*, 3851.
- (34) Rosink, J. J. W. M.; Blauw, M. A.; Geerligs, L. J.; van der Drift, E.; Rouseeuw, B. A. C.; Radelaar, S. *Opt. Mater.* **1998**, *9*, 416.
- (35) Onipko, A. I.; Berggren, K. F.; Klymenko, Y. O.; Malysheva, L. I.; Rosink, J. J. W. M.; Geerligs, L. J.; van der Drift, E.; Radelaar, S. *Phys. Rev. B* **2000**, *61*, 11118.
- (36) Porath, D.; Cuniberti, G.; Di Felice, R. Charge transport in DNA-based devices. In *Long-Range Charge Transfer in DNA II*; Springer: Berlin, 2004; Vol. 237, p 183.
- (37) Xu, M. S.; Tsukamoto, S.; Ishida, S.; Kitamura, M.; Arakawa, Y.; Endres, R. G.; Shimoda, M. *Appl. Phys. Lett.* **2005**, *87*.
- (38) Schonenberger, C.; Sondaghuethorst, J. A. M.; Jorritsma, J.; Fokkink, L. G. J. *Langmuir* **1994**, *10*, 611.
- (39) Palik, E. D. *Handbook of Optical Constants of Solids*; Academic Press: Orlando, 1985.
- (40) He, J.; Lin, L.; Zhang, P.; Lindsay, S. *Nano Lett.* **2007**, *7*, 3854.
- (41) Movileanu, L.; Benevides, J. M.; Thomas, G. J., Jr. *Nucleic Acids Res.* **2002**, *30*, 3767.
- (42) Case, D. A.; Darden, T. A.; Cheatham, T. E.; Simmerling, C. L.; Wang, J.; Duke, R.; Luo, R.; Merz, K. M.; Wang, B.; Pearlman, D. A.; Tsui, V.; Crowley, M.; Brozell, S.; Gohlke, H.; Mongan, J.; Hornak, V.; Cui, G.; Beroza, P.; Schafmeister, C.; Caldwell, J. W.; Ross, W. S.; Kollman, P. A. *AMBER 8*; University of California: San Francisco, 2004.
- (43) Perez, A.; Marchan, I.; Svozil, D.; Sponer, J.; Cheatham, T. E., 3rd; Laughton, C. A.; Orozco, M. *Biophys. J.* **2007**, *92*, 3817.
- (44) Frisch, M. J.; Trucks, G. W.; Schlegel, H. B.; Scuseria, G. E.; Robb, M. A.; Cheeseman, J. R.; Montgomery, J. A., Jr.; Vreven, T.; Kudin, K. N.; Burant, J. C.; Millam, J. M.; Iyengar, S. S.; Tomasi, J.; Barone, V.; Mennucci, B.; Cossi, M.; Scalmani, G.; Rega, N.; Petersson, G. A.; Nakatsuji, H.; Hada, M.; Ehara, M.; Toyota, K.; Fukuda, R.; Hasegawa, J.; Ishida, M.; Nakajima, T.; Honda, Y.; Kitao, O.; Nakai, H.; Klene, M.; Li, X.; Knox, J. E.; Hratchian, H. P.; Cross, J. B.; Bakken, V.; Adamo, C.; Jaramillo, J.; Gomperts, R.; Stratmann, R. E.; Yazyev, O.; Austin, A. J.; Cammi, R.; Pomelli, C.; Ochterski, J. W.; Ayala, P. Y.; Morokuma, K.; Voth, G. A.; Salvador, P.; Dannenberg, J. J.; Zakrzewski, V. G.; Dapprich, S.; Daniels, A. D.; Strain, M. C.; Farkas, O.; Malick, D. K.; Rabuck, A. D.; Raghavachari, K.; Foresman, J. B.; Ortiz, J. V.; Cui, Q.; Baboul, A. G.; Clifford, S.; Cioslowski, J.; Stefanov, B. B.; Liu, G.; Liashenko, A.; Piskorz, P.; Komaromi, I.; Martin, R. L.; Fox, D. J.; Keith, T.; Al-Laham, M. A.; Peng, C. Y.; Nanayakkara, A.; Challacombe, M.; Gill, P. M. W.; Johnson, B.; Chen, W.; Wong, M. W.; Gonzalez, C.; Pople, J. A. *Gaussian 03*, revision E.01; Gaussian, Inc.: Wallingford, CT, 2003.
- (45) Zhao, Y.; Schultz, N. E.; Truhlar, D. G. *J. Chem. Theor. Comput.* **2006**, *2*, 364.
- (46) Duguid, J. G.; Bloomfield, V. A.; Benevides, J. M.; Thomas, G. J., Jr. *Biophys. J.* **1996**, *71*, 3350.
- (47) Nunez, M. E.; Barton, J. K. *Curr. Opin. Chem. Biol.* **2000**, *4*, 199.
- (48) Dedachi, K.; Natsume, T.; Nakatsu, T.; Tanaka, S.; Ishikawa, Y.; Kurita, N. *Chem. Phys. Lett.* **2007**, *436*, 244.
- (49) Tsukamoto, T.; Ishikawa, Y.; Natsume, T.; Dedachi, K.; Kurita, N. *Chem. Phys. Lett.* **2007**, *441*, 136.
- (50) Coropceanu, V.; Cornil, J.; da Silva, D. A.; Olivier, Y.; Silbey, R.; Bredas, J. L. *Chem. Rev.* **2007**, *107*, 926.
- (51) Bloch, A. N.; Weisman, R. B.; Varma, C. M. *Phys. Rev. Lett.* **1972**, *28*, 753.
- (52) Holczer, K.; Gruner, G.; Mihaly, G.; Janossy, A. *Solid State Commun.* **1979**, *31*, 145.
- (53) Kutnjak, Z.; Filipic, C.; Podgornik, R.; Nordenskiold, L.; Korolev, N. *Phys. Rev. Lett.* **2003**, *90*, 098101.
- (54) Ortman, F.; Hannewald, K.; Bechstedt, F. *J. Phys. Chem. B* **2009**, *113*, 7367.
- (55) Sewell, G. L. *Polarons and Excitons*; Plenum Press: New York, 1962.
- (56) Emin, D. *Handbook of Conducting Polymers*; Dekker: New York, 1986.
- (57) Grozema, F. C.; Tonzani, S.; Berlin, Y. A.; Schatz, G. C.; Siebbeles, L. D.; Ratner, M. A. *J. Am. Chem. Soc.* **2008**, *130*, 5157.
- (58) Valis, L.; Wang, Q.; Raytchev, M.; Buchvarov, I.; Wagenknecht, H. A.; Fiebig, T. *Proc. Natl. Acad. Sci. U.S.A.* **2006**, *103*, 10192.
- (59) Cleveland, C. L.; Barnett, R. N.; Bongiorno, A.; Joseph, J.; Liu, C. S.; Schuster, G. B.; Landman, U. *J. Am. Chem. Soc.* **2007**, *129*, 8408.
- (60) Takada, T.; Fujitsuka, M.; Majima, T. *Proc. Natl. Acad. Sci. U.S.A.* **2007**, *104*, 11179.
- (61) Osakada, Y.; Kawai, K.; Fujitsuka, M.; Majima, T. *Nucleic Acids Res.* **2008**, *36*, 5562.
- (62) Roy, S.; Vedala, H.; Roy, A. D.; Kim, D. H.; Doud, M.; Mathee, K.; Shin, H. K.; Shimamoto, N.; Prasad, V.; Choi, W. B. *Nano Lett.* **2008**, *8*, 26.
- (63) Berashevich, J.; Chakraborty, T. *J. Chem. Phys.* **2008**, *128*.